Published in AJSE, Vol: 25, Issue:1
Received on 8th June 2025
Revised on 21st August 2026
Published on 31st August 2026

AIUB JOURNAL OF SCIENCE AND ENGINEERING
ISSN: 1608 - 3679 (print) 2520 - 4890
(Onlinehttps://doi.org/10.53799/gy5g0f03

Coati Optimized RBFNN MPPT-Controlled Interleaved DuoCore High-Gain Converter for PV Grid Integration

S. Suganya[1*], S. Thirunavukkarasu[2], S. Siddik[3], C. Arulkumar[4]

***Abstract*—The necessity for effective Photovoltaic (PV) power integration with dependable grid support has been brought to light by the rising demand for clean and sustainable energy. However, issues including variable solar radiation, erratic voltage and ineffective energy storage management frequently lower system performance. Therefore, this paper proposes a grid-connected PV architecture with a Coati Optimisation Algorithm (COA) tuned Radial Basis Function Neural Network (RBFNN) based MPPT for precise and quick maximum power extraction to address these problems. An interleaved DuoCore high-gain converter is deployed to boost up the PV output with less ripple. The system uses a Bidirectional DC–DC (BDC) converter to control battery charging and discharging for steady energy flow. A three-phase Voltage Source Inverter (VSI) controlled via a Proportional Integral (PI) regulator guarantees synchronized grid integration by preserving active and reactive power balance. The outcomes from MATLAB/Simulink ensures that the proposed architecture is appropriate for grid stability and dependability by accomplishing power conversion efficiency of (96%) and tracking accuracy (99.2%) compared to the other traditional strategies.**

***Keywords*—Photovoltaic, COA-RBFNN, MPPT, interleaved DuoCore high-gain converter, battery.**

I. Introduction

THE significant challenges associated with ecological change and global warming created by greenhouse gas emissions have garnered attention during the last few decades [1]. The rising demand for clean and sustainable energy has led to the large-scale use of renewable energy systems to reduce dependence on fossil fuels [2]. For the production of power, Renewable Energy Sources (RES) such as wind, solar and FC fuel cells are used. However, in contrast to other sources solar system performs better as it produce energy by absorbing the sunlight. It is possible to link solar cells in series to raise their output voltage [3]. Nevertheless, owing to shadow effect, this model fails to reach maximize and consistent output voltage [4]. Applying a DC–DC converter is to address this challenge. For connecting minimal to high voltage sources, boost DC–DC converters are necessary as seen in Fig. 1 [5]. Conventional boost converter (CBC) is frequently chosen due to its ease of use. In some situations, its efficacy is limited by voltage gain and switch stress [6]. Due of these difficulties, research into alternate designs to improve efficiency and performance has increased. Several techniques are used to create high-step-up converters, interleaving converters [7], voltage multiplier cells (VMC), Coupled Inductors (CI), Switched Capacitors (SC), Switched Inductors (SI), and cascade methods. Researchers have already looked into combining these methods to create novel designs for converters. They greatly maximize an efficiency of power conversion systems by combining several different strategies. To achieve high voltage gain, an Active SI structure is coupled with SC cells in [8]. Switch overvoltage exceeds theoretical predictions in ASL-based converters, however, because of oscillations brought on by the interplay between parasitic capacitance and circuit inductance. RC snubbers lessen these impacts and raise system expenses. In [9], a CI ultrahigh step-up quadratic boost converter is proposed, hard-switching performance, high voltage stresses problems have a major effect on conversion efficiency. High voltage gain is achieved in [10] by a modified SC and SI network with a VM. Its dependence on very high-duty cycles, however, degrades efficiency, lowers power density and increases conduction and switching losses. In [11], the interleaved structure is examined in conjunction with sophisticated step-up converter techniques. To enhance voltage gain, a CI-based high-gain QBC utilising multi-winding CIs and VMCs is merged with interleaving in [12]. Nevertheless, results in voltage spikes and a rise in leakage current. Interleaved QBC and CBC are combined in [13] to create a sophisticated architecture. Due to the additional components, this complexity raises the size and weight of system, makes implementation more difficult and raises overall costs. Table I compares the structural features and parameters of DuoCore converter to the most closely related high step-up DC-DC converters described in the literature.

TABLE I
Comparison of Proposed Converter with Existing Converters

Feature	Ref. [8]	Ref. [10]	Ref. [12]	Proposed
CI	Yes	Yes	Yes	Yes
Interleaved Structure	Yes	Yes	No	Yes

S. Suganya is an Assistant Professor in the Department of Electrical and Electronics Engineering, Paavai Engineering College, Namakkal, Tamil Nadu, India – 637018. E-mail: suganyasugas51@gmail.com, Orcid ID: 0000-0003-2642-7208
S. Thirunavukkarasu is an Associate Professor in the Department of Electrical and Electronics Engineering, Paavai Engineering College, Namakkal, Tamil Nadu, India – 637018. E-mail: thirunavuspt5@gmail.com
S. Siddik is an Assistant Professor in the Department of Electrical and Electronics Engineering, Paavai Engineering College, Namakkal, Tamil Nadu, India – 637018. E-mail: rssiddik@gmail.com
C. Arulkumar is an Associate Professor in the Department of Electrical and Electronics Engineering, Paavai Engineering College, Namakkal, Tamil Nadu, India – 637018. E-mail: carulme@gmail.com

SC	Yes	N0	Yes	Yes
VMC	No	Yes	Yes	Yes
Voltage Stress Reduction	Partial	Partial	Moderate	Significant
Voltage Gain	High	High	High	Higher
Component Count	High	Moderate	High	Reduced
Novel Structural Feature	Existing	Existing	Existing	New DuoCore topology with optimized capacitor–coupled inductor configuration

For high-voltage, the proposed interleaved DuoCore High-Gain Converter offers a structurally well and functional solution. Previous converters use CI, SC, and VMC; however, the proposed DuoCore converter differs by introducing a unique arrangement of the dual-core CI and clamp capacitor network, resulting in enhanced voltage gain, lower switch voltage stress, and improved conversion efficiency.

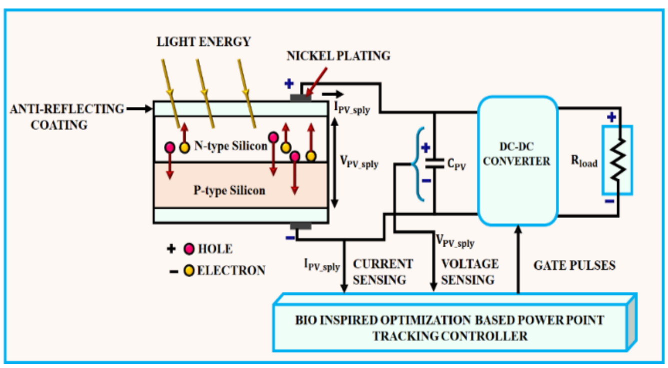

Fig. 1. Simple model view of PV based grid system.

Finding the global peak with a fixed step size is challenging with the current MPPT techniques [14]. The issues with the fixed step size MPPT technique have been addressed by the introduction of AI techniques. Variable step size in incremental conductance based on fuzzy logic performed better, but not in settling time [15]. Although the ANN-based MPPT provided superior results to the traditional MPPT, tracking and conversion efficiency remain low [16]. The improved dynamic flexibility of AI-based controllers is demonstrated by comparing ANFIS-based MPPT methods with conventional methodologies. It is verified in [17] that ANFIS models maintain dependable performance even in the face of sudden environmental changes, in addition to converge more quickly. Although, the training time is higher and optimal tuning is crucial for improving the MPP outcomes. The RMSE error is forecasted and minimised via PSO that shows good efficiency, rapid convergence and sufficient performance in partially shaded conditions [18]. In [19] developed a combination of an MPPT operator based on ABC and ANFIS. The ABC has been used to modify the ANFIS membership function. For solar plants that run in partial shade, the author in [20] offer an ABC and an optimised P&O algorithm. The GMPP is calculated using the ABC, and it is further determined using P&O. Even with improvements in MPPT techniques, current methods frequently find it difficult to adjust to variations in ambient temperature and sunshine intensity, which results in less than ideal performance and lower energy yield. The identified research gap emphasises the necessity of a new MPPT method that maximize overall performance of grid-connected PV systems and get around the drawbacks of conventional systems. Henceforth, proposed study deploys a novel bio inspired optimization for optimal tuning of intelligent approach.

A. Key contributions

- To create a PV-based power generation system that effectively extract energy in a several of ecological situations.
- To use an RBFNN-based MPPT technique that is COA-optimized to track MPP quickly and accurately.
- To create a high-gain interleaved DuoCore converter that guarantees high voltage gain though lowering current ripple and increasing efficiency.
- To incorporate BDC converter to enable efficient battery charging and discharging, permitting load balancing and energy storage.

II. Proposed System Model

A PV array uses solar energy to generate electricity as displayed in Fig. 2. In order to increase PV voltage to a steady DC-link level while reducing ripples and improving conversion efficiency, an interleaved DuoCore high-gain converter. The system uses RBFNN-based MPPT controller that has been adjusted by the Coati optimisation algorithm to guarantee maximum energy extraction under various environmental circumstances. A PWM generator converts the precise reference signals produced by this intelligent controller from PV voltage and current into switching pulses for designed converter.

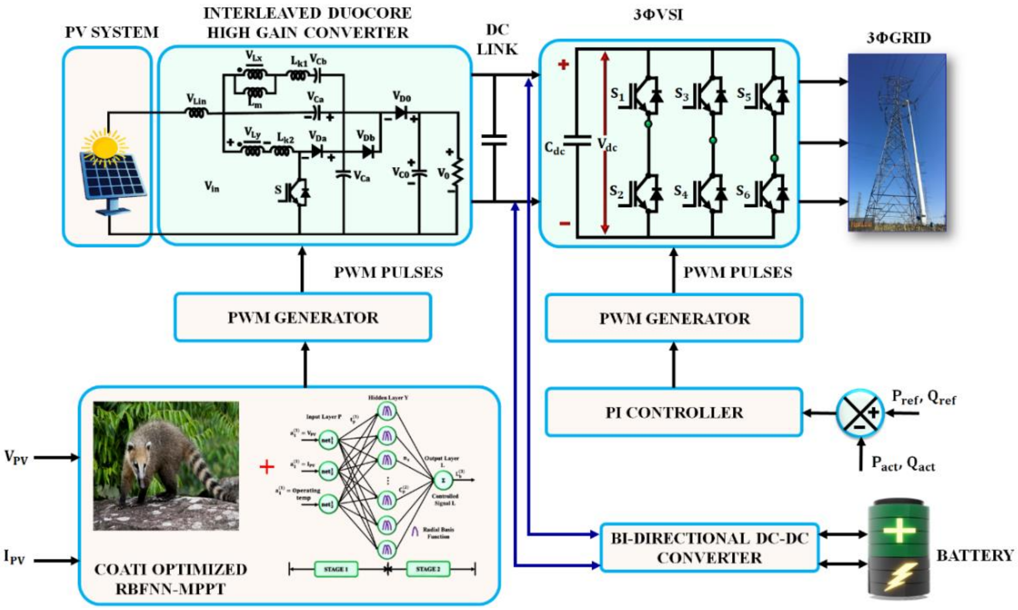

Fig. 2. Schematic diagram of advanced converter with MPPT for grid system.

To facilitate energy storage and supply balancing, a BDC converter is incorporated with DC-link to control the associated battery's charging and discharging. A three-phase VSI transforms controlled DC-link voltage into utility-synchronized AC power for grid integration. For preserving grid stability and power quality, inverter is measured via a PI controller that compares the actual active and reactive power with its reference values using PWM signals. Reliable renewable energy use is made possible by this coordinated operation, which also provides grid assistance and effective storage.

A. Modelling of PV model

A single-diode model approach of moderate complexity is deployed in this study to describe the PV device because it is a improved balance between simplicity and accuracy to represent the behaviours of PV device shown in Fig. 3. Output PV cell is indicated as:

$$I = I_{ph} - I_d - I_{sh} \tag{1}$$

Where, I_{ph}, I_d *and* I_{sh} stands photocurrent, diode current and shunt current (A).

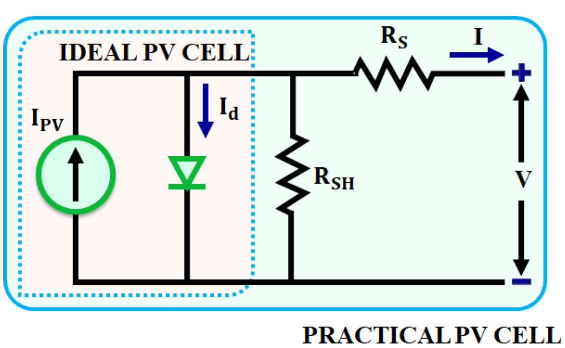

Fig. 3. Equivalent model of PV.

$$I = I_{ph} - I_0\left[exp\left(\frac{q(V+IR_S)}{nkT}\right) - 1\right] - \frac{V+IR_S}{R_{sh}} \tag{2}$$

Where, reverse current saturation in diode is specified as I_0, electron charge is stands as q , V denotes terminal voltage (V), n stands diode ideality factor, Boltzmann constant is refer as k and temperature (K) is denoted as T. R_s *and* R_{sh} stands series and shunt resistance (Ω). Moreover, the current PV module energy can't provide essential energy to grid system owing to the changes in temperature and intensity, so the proposed model aims to provide a novel Interleaved DuoCore High-Gain Converter to satisfy the grid system as discussed below.

B. Interleaved DuoCore High-Gain Converter

. Interleaved DuoCore High-Gain Converter structure, which consists of a single active switch, an input inductor to minimize input current ripple and a CI with inductors as displays in Fig. 4. Fig. 5(a) shows the fundamental waveforms of converter operation in CCM and 5(b) displays switching waveform of designed converter.

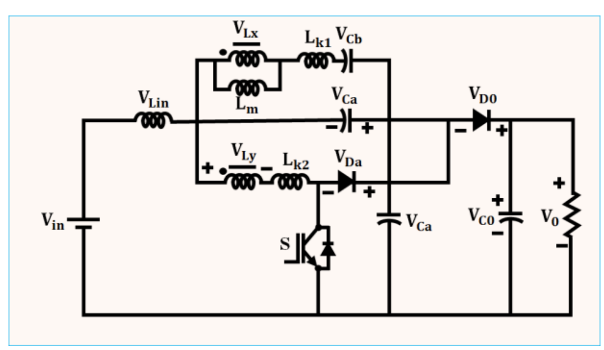

Fig. 4. Equivalent circuit of Interleaved DuoCore High-Gain Converter.

Mode 1: Switch S begins to conduct at this moment. Voltages are under reverse bias with diode D_o, while diode D_1 is conducting. The input inductor and secondary side of CI receive DC energy from the input source. Both inductances are charged, and currents iL_{in} and CI grow linearly. Capacitors $C_b$and C_c are discharged in this manner, clamping over secondary side of connected inductor and voltage of C_a. Consequently, the energy kept in connected inductor used to raise C_a voltage and the load gets energized by C_o.

Mode 2: S is turned off at this phase. Diodes D_o now begin to conduct, while voltage blocks diode D_1. The input inductance is discharged when stored energy in inductor L_{in} is given to couple inductor's magnetising inductance. It causes a linear increase in current. Additionally, $C_b$and C_c are charged by L_X. In this mode, the input voltage, input inducer and C_a are used to supply energy needed for load, raising the output voltage.

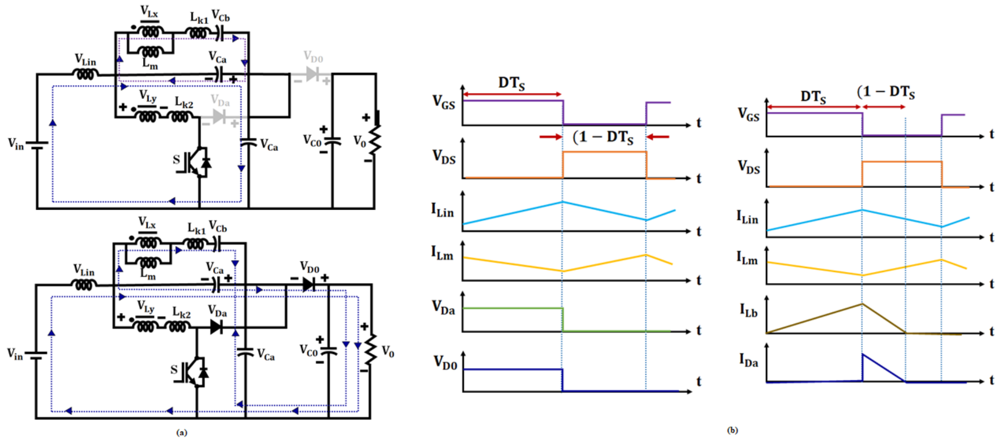

Fig. 5. (a) Modes of operation and (b) Switching state of converter.

For the converter to function in CCM, two distinct modes are consider. The following is an expression for the equations associated,

$$VL_{in} = V_{in} + V_{Ca} - V_{Cc} \tag{3}$$

As stated in mode 1 and 2, the voltages across inductors $L_X$and L_Y are computed.

$$VL_{in} = V_{Cb} - V_{Ca} \tag{4}$$

$$VL_{in} = V_{Cc} - V_{Ca} \tag{5}$$

The aforementioned equations reformulated when S is turned off in second mode.

$$VL_{in} = V_{Ca} + V_{in} - V_o \tag{6}$$

$$VL_X = V_o + V_{Cb} - V_{Ca} - V_{Ca} \tag{7}$$

$$VL_Y = V_o - V_{Ca} - V_{Ca} \tag{8}$$

For the L_{in}, L_X and L_Y, the voltage-second balance law is applied as follows:

$$\int_0^{DT_s} V_{LX(on)}dt + \int_0^{T_s} V_{LY(off)}dt = 0 \tag{9}$$

$$\int_0^{DT_s} VL_{in(on)}dt + \int_{DT_s}^{T_s} VL_{in(off)}dt = 0 \tag{10}$$

$$\int_0^{DT_s} V_{LY(on)}dt + \int_{DT_s}^{T_s} V_{LY(off)}dt = 0 \tag{11}$$

The capacitors C_a, $C_b$and C_c voltages found using (3) through (11) as:

$$V_{Ca} = \frac{V_o(D-1)^2 + V_{in}(2D-1)}{1-D} = \frac{n-D}{2n-1}V_o \tag{12}$$

$$V_{Cb} = \frac{D}{1-D}V_{in} = \frac{D(n-1)}{2n-1}V_o \tag{13}$$

$$V_{Cc} = \frac{V_{in}}{1-D} = \frac{(n-1)}{2n-1}V_o \tag{14}$$

In CCM operation, voltage gain is designed as follows:

$$M = \frac{V_o}{V_{in}} = \frac{2n-1}{(n-1)(1-D)} \tag{15}$$

The proposed converter performance is improved by generating needful energy to grid system and achieves higher conversion efficiency. Additionally, for improving converter performance, the voltage and current from PV has to be tracked with the MPPT techniques, hence the proposed model uses RBFNN based MPPT topology as deliberated below.

C. RBFNN-MPPT

RBFNN model is created in this work to identify the PV module's highest power point. The RBFNN is made up of three layers: input layer 1 (Layer-1), hidden radial basis layer 2, and output layer 3, as shown in Fig. 6.

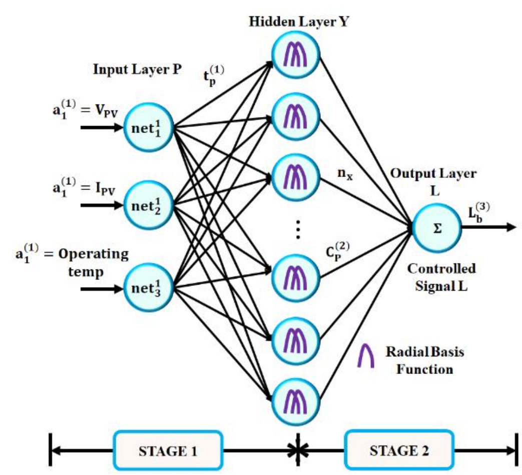

Fig. 6. Structure of RBFNN layer for MPPT.

Equations (16–18) explain the input layer $\left(net^{(1)}\right)$,

$$net\ value_v^{(1)} = t_v^1(g),\ \ here\ g = 1,2,3,\ldots\ldots,P \quad (16)$$

$$R_v^{(!)}(g) = f_v^{(1)}\left(net\ value_v^{(1)}(g)\right) = net_v^1(g), here\ g = 1,2,3,\ldots,P \quad (17)$$

Where, g denotes training sample index, P represents total number of training samples, v represents input neuron index.

Equations (18–19) reflect the hidden radial basis layer $\left(net^{(2)}\right)$,

$$net\ value_m^{(2)}(g) = -(\varepsilon - \psi_m)^T * \sum_r(\varepsilon - \psi_m) \quad (18)$$

$$C_k^{(2)}(g) = f_k^{(1)}\left(net_v^{(2)}(g)\right),\ \ here\ g = 1,2,3,\ldots P \quad (19)$$

Here, ε denotes input feature vector, ψ_m stands centre vector of the m^{th} RBF, and r stands Gaussian spread (width) parameter.

Equations (20)–(22) correspond to the output layer and error computation$\left(net^{(3)}\right)$.

$$net_1^{(3)} = \sum_k W_k * L_k^2\,(g),\ \ \ here\ g = 1,2,3\ldots P \quad (20)$$

$$g_s^{(3)}(g) = f_p^{(3)}\left(\left(net_p^3(g)\right)\right) = net_p^3(g), \quad (21)$$

$$Error = \sum_{i=1,2}^{m} \frac{1}{2}\left(E_{ref\ value} - E_{peak}\right) \quad (22)$$

Where, W_k represents t connection weight between the hidden layer and output layer, while L_k^2 denotes output of the k^{th} hidden neuron. E_{ref} denotes reference maximum power, and E_{peak} represents estimated maximum power obtained from the RBFNN.

D. Coati Optimization Algorithm

For effective MPPT, the RBFNN parameters are optimally tuned in this study using COA. Two basic natural behaviours of coatis are imitated to model the position updating process of candidate solutions (coatis) in COA such as,

- Hunting strategy when attacking iguanas (Exploration phase)
- Escape strategy from predators (Exploitation phase)

Therefore, the RBFNN weights and biases are tuned in two stages, allowing for a balance between local refinement for MPPT accuracy and global exploration of the solution space.

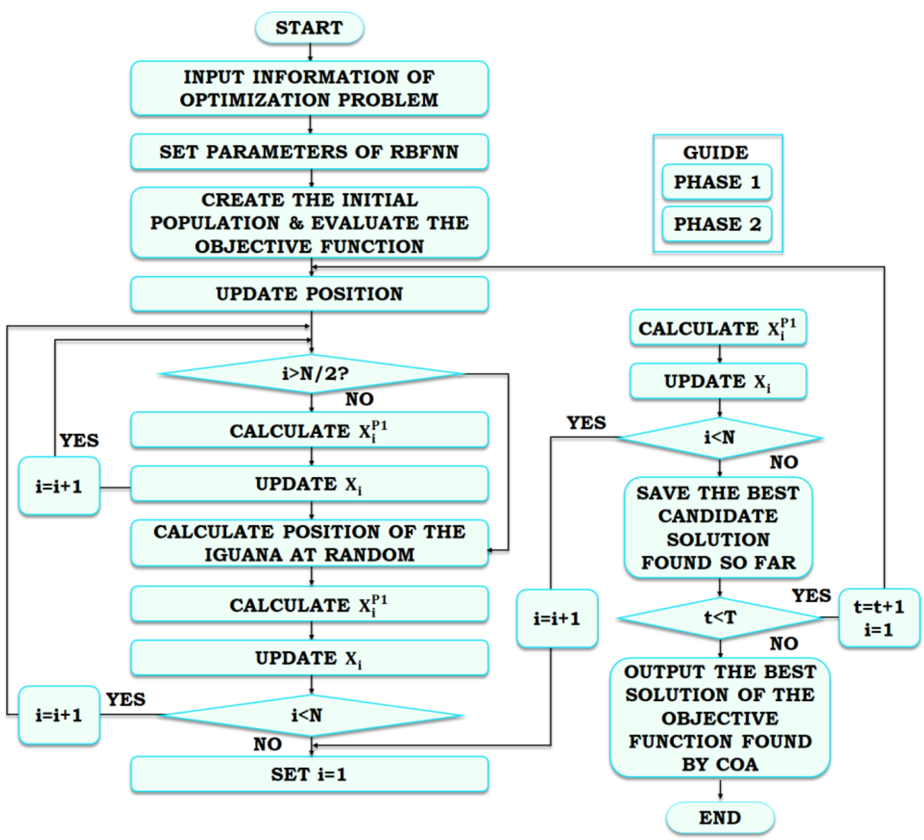

Fig. 7. Flowchart representation model of proposed MPPT model.

❖ ***Hunting strategy when attacking iguanas (Exploration phase):***

The method search broadly for ideal RBFNN parameter values (weights and biases) that maximise the MPPT efficiency with the aid of first phase, which reflects exploring behaviour of coatis. Here, some coatis wait below till the iguana falls, while others scale the tree to frighten it. New exploratory positions in search space result from this. The position of the iguana is believed to be the best-performing RBFNN configuration in the COA design, with the lowest MPPT error or greatest power extraction.

Position update of climbing coatis mathematically expressed as,

$$x_{i,j}^{P1} = x_{i,j} + r.\left(I_{iguana\,j} - I.x_{i,j}\right), \quad i = 1,2,\ldots,\left[\frac{N}{2}\right], j = 1,2,,,m \quad (23)$$

Here, $x_{i,j}^{P1}$ denotes Updated solution obtained during the exploration phase. $x_{i,j}$ stands decision variables, $I_{iguana\,j}$ represents position of iguana, r stands random number [0,1]. Iguana is positioned at random across RBFNN variable search space as,

$$I_{iguana}G_j = lb_j + r.\left(ub_j - lb_j\right), \; j = 1,2,\ldots.m \quad (24)$$

Here, $I_{iguana}G_j$ represents randomly generated iguana position during exploration, ub_j and lb_j stands upper and lower bound. Ground-level coatis adjust its placements in accordance with this random position as follows:

$$x_{i,j}^{P1} = \begin{cases} x_{i,j} + r.\left(I_{iguana}G_j - I.x_{i,j}\right), & F((I_{iguana}G) < F_i \\ x_{i,j} + r.\left(x_{i,j} - (I_{iguana}G_j\right), & else \end{cases}, i = \left[\frac{N}{2}\right] + 1,\ldots, \quad (25)$$

Here, F_i denotes objective function, N stands total population size. The modified position is only approved if it improves the MPPT objective function, which includes enhancing extracted power or decreasing tracking error.

$$X_i = \begin{cases} X_i^{P1}, & F_i^{P1} < F_i \\ X_i, & else \end{cases} \quad (26)$$

Where, X_i represents RBFNN parameter vector, F_i stands for MPPT error for the ith solution, r indicates random number [0, 1], lb_j and ub_j refers lower and upper bounds of parameters and I denotes integer randomly chosen from [1, 2].

❖ ***Escape strategy from predators (Exploitation phase)***

When avoiding predators, coatis try to localise their positions in the second phase as seen in Fig. 8, which is an example of exploitation behaviour. This makes it possible to attain high MPPT precision by fine-tuning RBFNN parameters close to potential solutions. As iterations increase the intensity of local search, the local boundaries get smaller.

$$lb_j^{local} = \frac{lb_j}{t}, ub_j^{local} = \frac{ub_j}{t}, \; t = 1,2,\ldots.,T \quad (27)$$

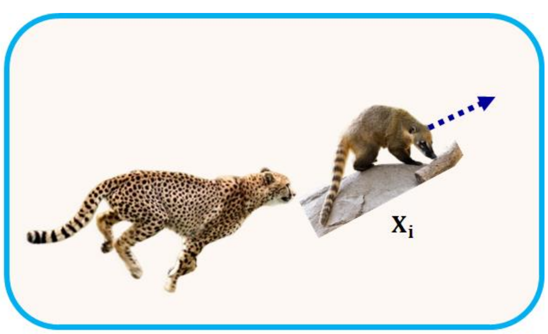

Fig. 8. Escaping strategy of coati.

The local update rule is defined as,

$$x_{i,j}^{P2} = x_{i,j} + (1-2r).\left(lb_j^{local} + r.\left(ub_j^{local} - lb_j^{local}\right)\right), \; i = 1,2,\ldots.N \quad (28)$$

Here, $x_{i,j}^{P2}$ denotes Updated solution obtained during the exploitation phase. The new position is retained if it get improved MPPT performance,

$$X_i = \begin{cases} X_i^{P2}, & F_i^{P2} < F_i \\ X_i, & else \end{cases} \quad (29)$$

Where, F_i^{P2} stands for MPPT error and t refers iteration counter. The behaviour of tuning RBFNN parameters are shown by the flowchart in Fig. 7.

E. BDC converter

When switch is in ON state, the BDC converter runs in boost mode, enhancing voltage to meet load demand. It operates in continuous operation mode. Fig. 9 shows schematic diagram of a BDC converter. Also, when the switch is in OFF position through step down operation, it functions as a battery charging mode. Equations that characterise this converter's dynamic model include

$$L = \frac{V_{DCref} \times (V_{in} - V_{out})}{I_{ripple} \times F_{sw} \times V_{in}} \quad (30)$$

$$C = \frac{I_{ripple}}{(8 \times F_{sw} \times V_{ripple})} \quad (31)$$

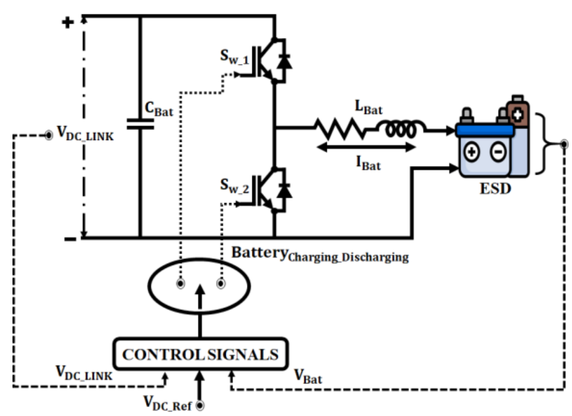

Fig. 9. Circuit of BDC converter.

The incorporation of battery system ensures continuous energy supply to grid system in the event of power shortage from PV.

F. Grid Synchronization

A grid-connected PV system's inverter output needs to be in phase with utility grid involves voltage, frequency and phase angle for dependable operation. Synchronisation guarantees the effective delivery of the injected power without resulting in instability or problems with power quality. A Phase-Locked Loop (PLL) and a PI controller are used in the system to adjust three-phase VSI to correspond with the grid conditions. In α-β reference frame, the rapid powers are derived as:

$$P = \frac{3}{2}\left(V_\alpha I_\alpha + V_\beta I_\beta\right) \quad (32)$$

$$Q = \frac{3}{2}\left(V_\alpha I_\beta - V_\beta I_\alpha\right) \quad (33)$$

Where, V_α, V_β and I_α, I_β are obtained by Clarke transformer of three phase voltages and currents. PI controller minimizes an error over reference values (P_{ref}, Q_{ref}) and actual values (P_{act}, Q_{act}), generating control signals for PWM generator. This ensures that the inverter injects the desired amount of active power to grid and maintaining reactive power support for voltage stability.

III. Results And Discussion

The proposed work is evaluated by providing outcomes from MATLAB/Simulink. The outcomes involves various test conditions for showing the prominence of proposed model. Additionally, the comparison performance of various metrics are done in the end of this section. Following Table II displays a parameter specification for designed model.

TABLE II
PARAMETER SPECIFICATION OF PROPOSED MODEL

Solar PV System			
Parameters	**Values**	**Parameters**	**Values**
Power Rating	20kW	*Open circuit Voltage*	37.25V
Short circuit Current	8.95 A	*Series and Parallel connected Solar cell*	11, 3
Maximum Voltage	29.95V	Maximum Current	8.35A
Interleaved DuoCore high-gain converter			
L_m, L_k		$45\mu F$	
L_x, L_y		$4.7\mu H$	
C_a, C_b		$22\mu F$	
C_o		$2200\mu F$	
Switching Frequency		100kHz	

Case 1: PV performance under constant condition

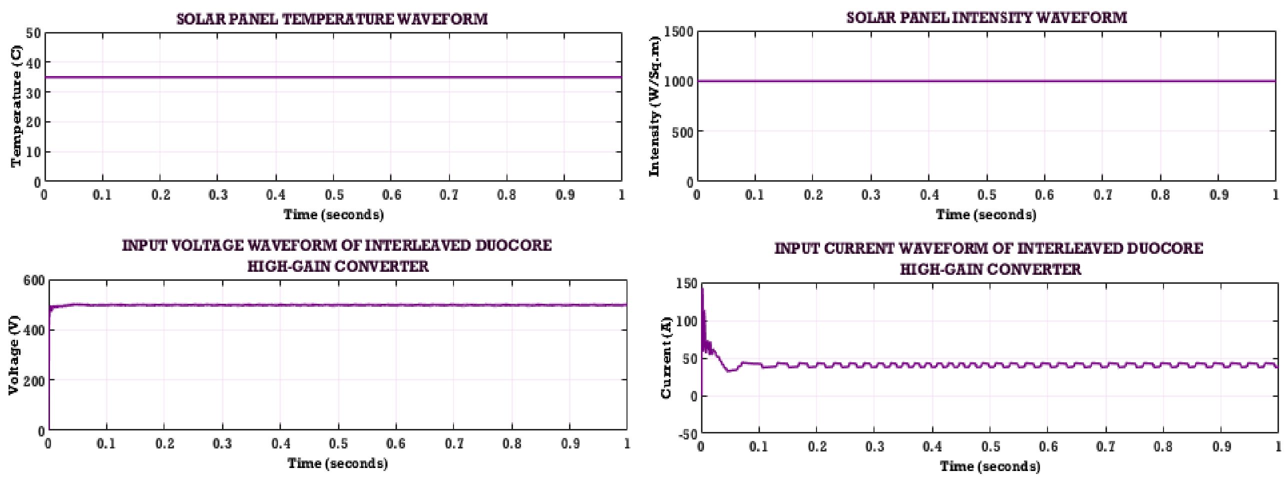

Fig. 10. PV system performance under case 1.

In the case of constant condition, thermal stability is ensured by maintaining the solar panel temperature at $25\,°C$ for the duration as displays Fig. 10. A constant irradiance of 1000 W/m^2 is maintained, which is the standard test condition. The interleaved DuoCore high-gain converter's input voltage smooth convergence to about 500V. Also, current waveform exhibits the system's capacity to suppress transients under this consistent environment by beginning with slight oscillations and maintained at 40A.

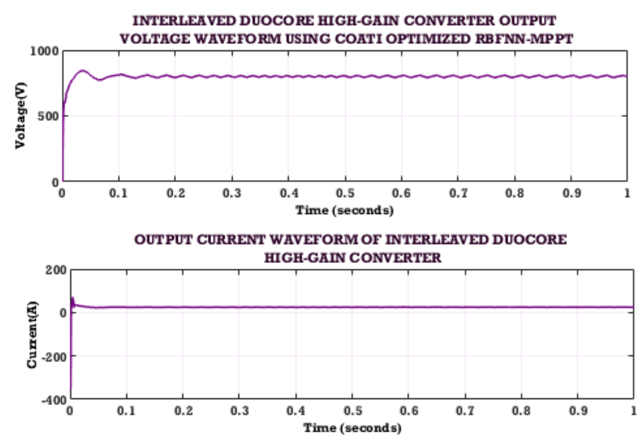

Fig. 11. Output voltage and current outcomes under constant scenario.

The efficiency of COA-optimized RBFNN-MPPT in sustaining high voltage gain is demonstrated by the converter's output, which generates a regulated voltage waveform that rises fast and stabilises near 800V as displayed in Fig. 11. Output current correspondingly stabilises at about 24A, guaranteeing a steady power supply to the grid free from oscillatory distortion.

Case 2: PV performance under varying condition

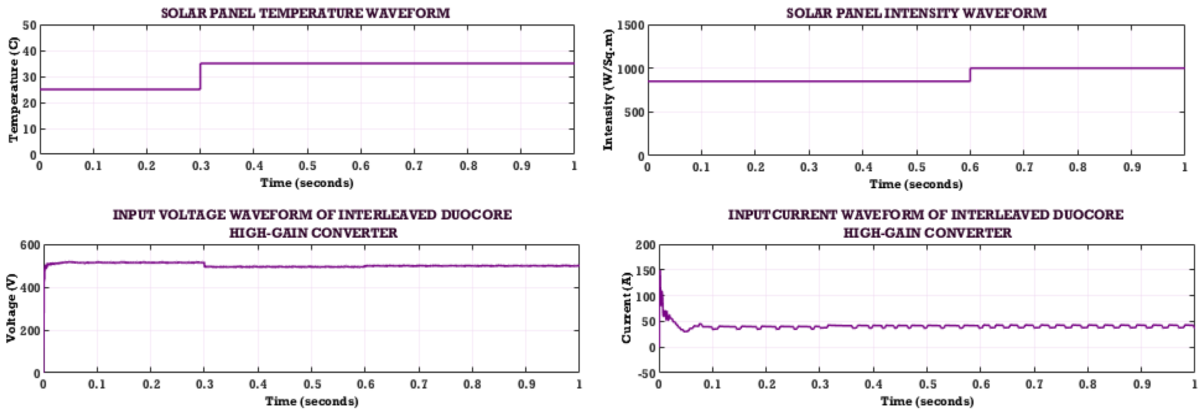

Fig. 12. PV system performance under case 2.

The temperature of solar panels stays at $25°C$ at first when PV system is subjected to dynamic changes, but at about 0.3s, it abruptly rises to $35°C$ and maintains continually. The irradiance also shows a sudden drop from $800\,W/m^2$ to $1000\,W/m^2$ owing to the changes in sun intensity. The input reactions of the converter are changed by these environmental changes. The interleaved DuoCore high-gain converter's input voltage varies but soon settles at about 500V, indicating good adaption. During the transition, the input current experiences a disruption and within 0.1s, it maintains at 40A as seen in Fig. 12.

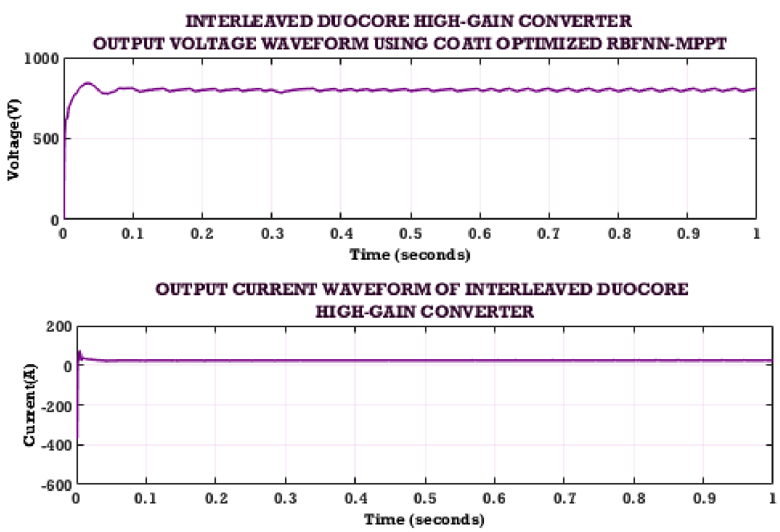

Fig. 13. Output voltage and current under varying scenario.

Despite environmental variation, the converter effectively controls an output side voltage about 800 V, exhibiting slight dips during variation before swiftly rebounding displayed in Fig. 13. The output current also briefly decreases before stabilising at 24A, demonstrating that COA optimized RBFNN-MPPT ensures dependable power delivery while offering robust resilience against environmental disruptions.

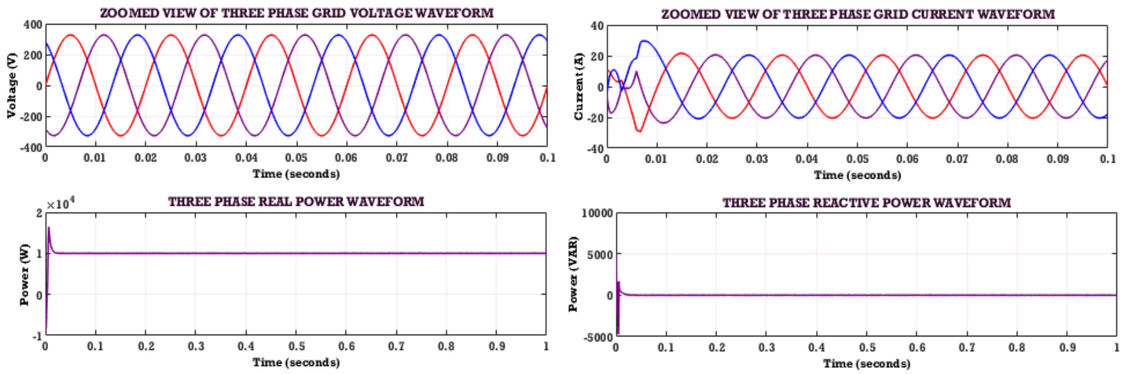

Fig. 14. Grid performance.

The three-phase grid voltage waveform's zoomed view verifies a balanced sinusoidal profile with a peak amplitude of about ±380V per phase, maintaining in synchronized with the grid standard. With the right phase alignment, the matching three-phase current waveform likewise shows sinusoidal behaviour, guaranteeing steady grid interaction. With a nearly constant delivery, the real power profile indicates that the integrated PV–battery system provides the grid with consistent active power. In the meantime, the reactive power waveform stabilises near negligible value, confirming efficient power factor correction and guaranteeing the grid has little reactive load as seen in Fig. 14.

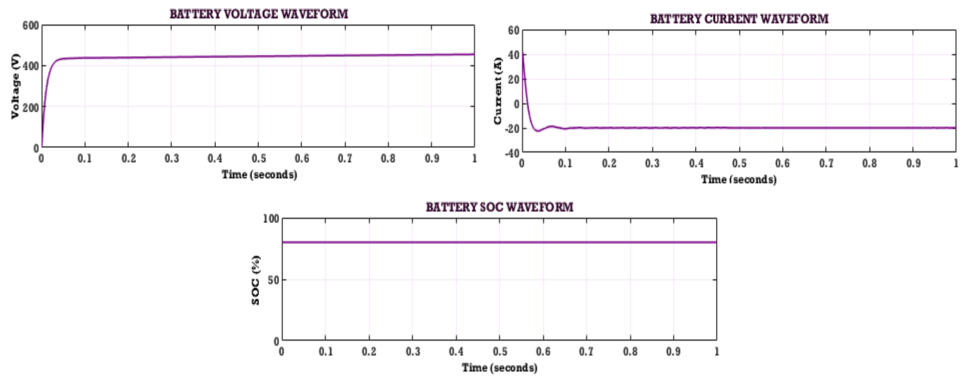

Fig. 15. Battery performance.

The battery voltage increases and stabilises near 420V under normal circumstances, signifying that it is ready to provide energy. As seen by the battery current's first transient charging/discharging behaviour before fast settling close to -20A. There is no discernible energy draw from storage during this time, as the battery's SoC waveform in Fig. 15 stays steady at 80%. This demonstrates how the battery is maintained as a backup source during regular operation, with the PV and converter handling the primary supply. This ensures a longer battery life and effective system management.

Case 3: Partial Shading

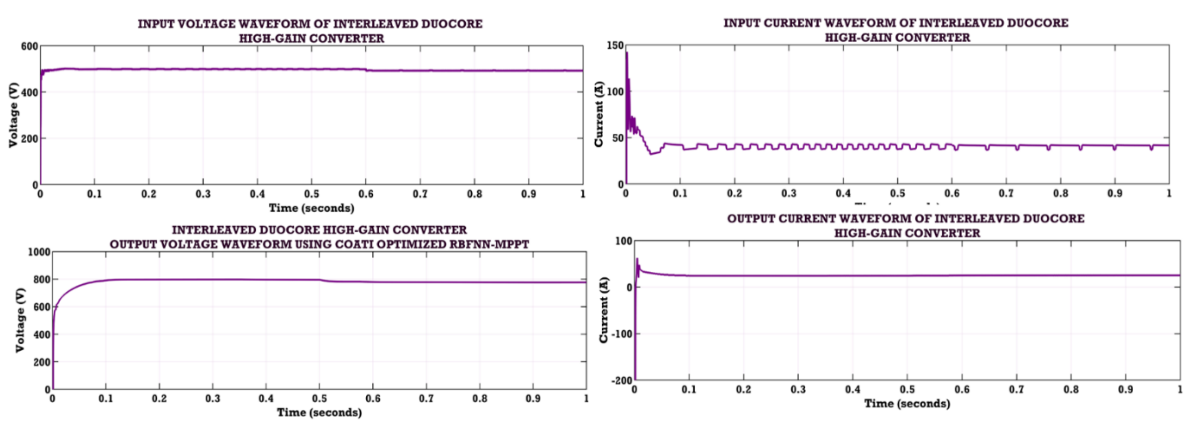

Fig. 16. Input and output waveforms under partial shading.

Fig. 16 depicts input and output voltage and current characteristics of Interleaved DuoCore High-Gain Converter under partial shade conditions. When the irradiance varies due to partial shading, there is a brief transient response lasting approximately 0.5 seconds. The proposed COA-RBFNN-based MPPT quickly detects and resumes stable operation. The output voltage remains close to 800 V, and the output current settles quickly with minimum fluctuations. These results show that the suggested controller is effective at guaranteeing stable voltage regulation and efficient power extraction in partial shade conditions.

Case 4: PV System cut-off at 0.45s, with Battery Powering grid

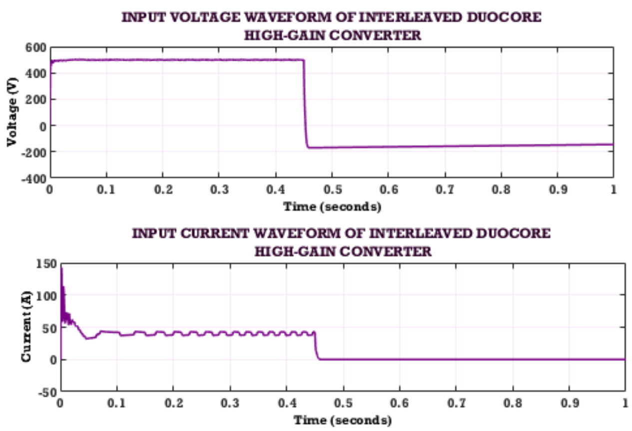

Fig. 17. PV performance under shutdown condition.

The interleaved DuoCore high-gain converter input profiles clearly show PV system cut-off at 0.45s signified in Fig. 17. After disconnecting the PV source, the input voltage abruptly drops after first stabilising at 500 V. In a similar way, the input current begins at about 150A and quickly drops after cut-off, indicating total PV contribution loss.

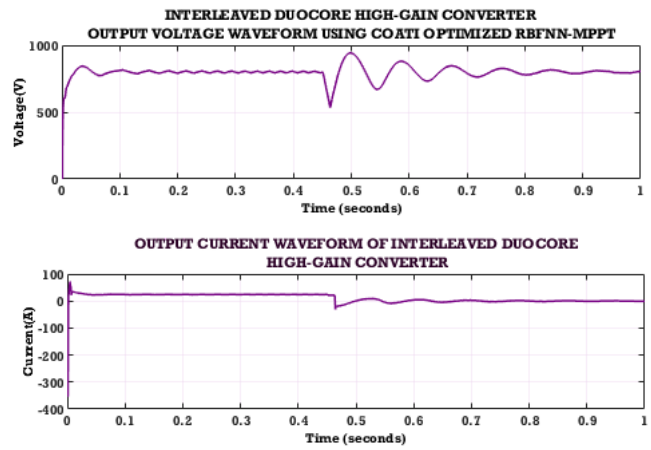

Fig. 18. Converter performance under case 4 condition.

Although a disturbance and little oscillation occur at the shutdown instant, the converter's output voltage is still controlled around 800V despite this cut-off, indicating effective voltage support under transitory interruption. During cut-off, the equivalent output current waveform, which initially stable at about 100A, similarly briefly distorts but soon stabilises to guarantee continuous load current in Fig. 18.

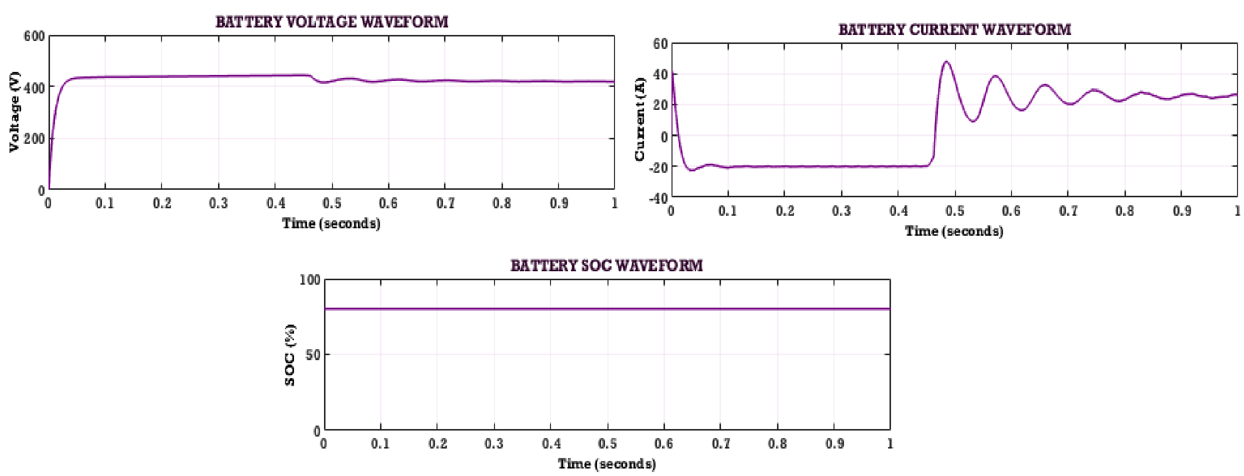

Fig. 19. Battery model outcomes under PV cut-off condition.

The battery takes over to continue power transmission in the event that the PV system disconnects. Battery voltage increases and stabilises near 420V, indicating that it is actively supporting the grid supply. After 0.45s, the battery current first drops, rises noticeably to around 30A with waves as it makes up for the lack of PV input as illustrated in Fig. 19. The energy is extracted during the brief simulation period, as indicated by SoC remaining almost constant at 80%. This demonstrates that the battery system has enough capacity to withstand unexpected PV shutdowns without experiencing appreciable depletion.

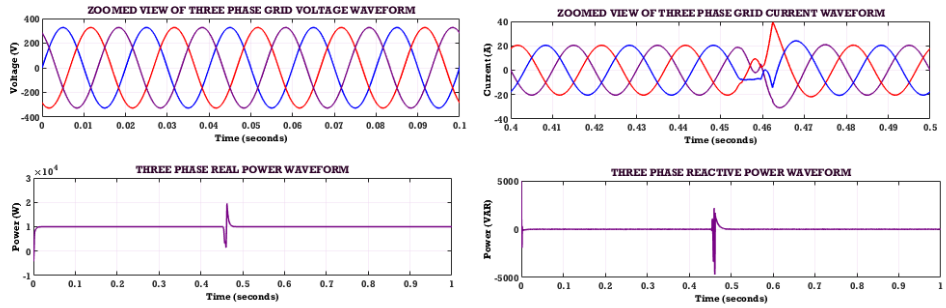

Fig. 20. Grid performance under case 4 condition.

The three-phase grid voltage waveform in Fig. 20 confirms voltage stability during Case 4 operation by maintaining a steady sinusoidal shape with peak values of about ±380V. Even though the three-phase current waveform is primarily sinusoidal, there is a slight disruption at 0.45s, which is when the PV system cut-off occurs. Strong grid synchronisation is demonstrated by the current waveform's rapid recovery to a balanced sinusoidal shape in spite of this transient. A slight decrease is seen at the cut-off instant before it stabilises again, indicating the transfer of power supply responsibility from PV to the battery. In such case, three-phase actual power stays constant and eliminated reactive power stays over the period, with a brief increase during the PV disconnection.

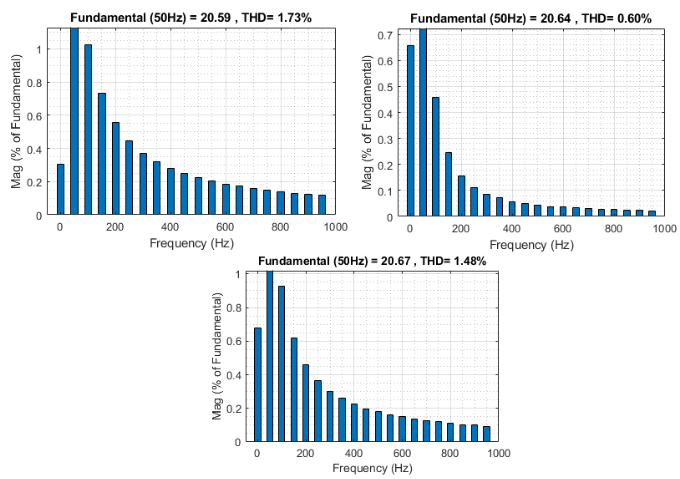

Fig. 21. THD performance for the proposed model of (R, Y and B phases).

THD analysis shows values of 1.73% (R phase), 0.60% (Y phase), and 1.48% (B phase), confirming outstanding power quality across all three phases demonstrated in Fig. 21. This demonstrates smooth sinusoidal current injection and extremely little harmonic distortion. Thus, even during PV cut-off transitions, dependable power regulation is guaranteed by proposed RBFNN-MPPT-controlled interleaved DuoCore converter.

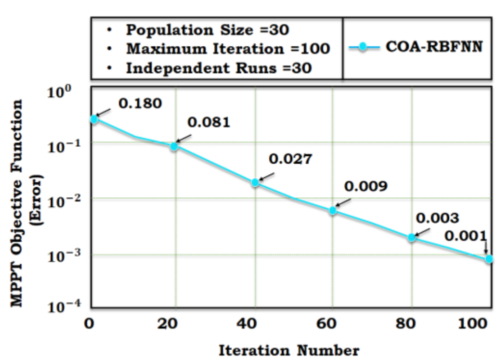

Fig. 22. Convergence characteristics of the developed COA-RBFNN algorithm.

Fig. 22 shows the convergence properties of the proposed COA-RBFNN algorithm. COA's efficient exploration ability results in a fitness value rapid reduction in initial iterations, and fitness value gradually approaches the optimal solution in the exploitation phase. The convergence curve demonstrates the rapid convergence speed and stable optimisation performance of the proposed algorithm.

A. Comparative analysis

TABLE III
COMPARISON OF EXISTING CONVERTER EFFICIENCY

Converter models	Efficiency value (%)
Interleaved DC-DC converter [6]	92.13
High step up converter with CI [7]	93.28
High step-up [8]	95.12
Proposed converter	**96**

With an efficiency of 96% in Table III, proposed converter outperformed the current devices documented in [6, 7] and [8]. The values mentioned in Refs. [6–8] are adapted from their respective publications and are obtained under different converter configurations and operating conditions. This confirms its efficacy for PV-assisted grid applications by showcasing its superior ability to achieve maximum power conversion with decreased losses.

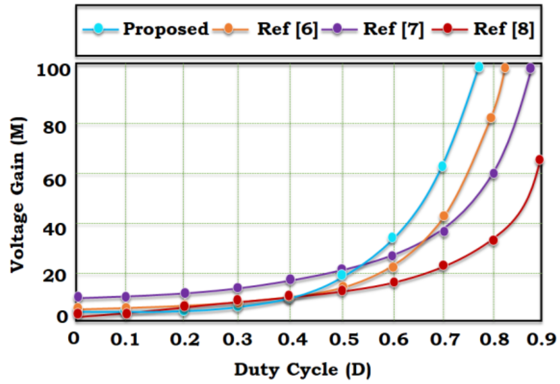

Fig. 23. Evaluation of Gain vs Duty Cycle

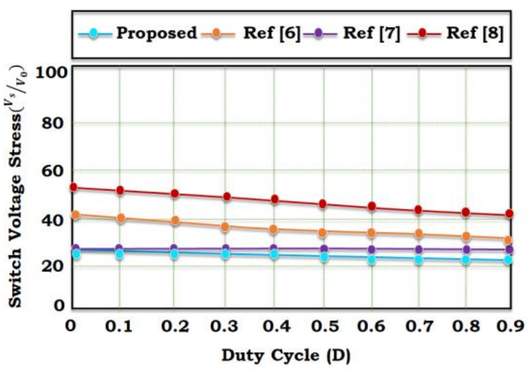

Fig. 24. Evaluation of voltage stress on switch

Fig. 23 shows voltage gain vs duty cycle of interleaved DuoCore high gain converter and existing converter. Voltage gain increases in proportion to the duty cycle, illustrating proposed converter's excellent step-up capacity. Fig. 24 displays voltage stress of proposed converter and existing. The reduced voltage stress across the power switches and diodes increases converter efficiency and allows for the use of lower-rated components.

TABLE IV
Converter efficiency under same condition

Converter Topology	Interleaved Boost	Proposed
PV Rating (kW)	20	20
Output Voltage (V)	800	800
Switching Frequency (kHz)	100	100
Irradiance (W/m²)	1000	1000
Temperature (°C)	25	25
Output Power (kW)	20	20
Efficiency (%)	93.1	96

Table IV shows comparison of different DC-DC converter at the same working condition. Proposed Interleaved DuoCore High-Gain Converter achieves an excellent conversion efficiency of 96.0% while maintaining the required voltage gain and output power.

TABLE V
Tracking performance efficiency under same condition and converter

Converter	Proposed Converter			
MPPT	P&O	INC	RBFNN	COA-RBFNN
PV Rating (kW)	20	20	20	20
Switching Frequency (kHz)	100	100	100	100
Irradiance (W/m²)	1000	1000	1000	1000
Temperature (°C)	25	25	25	24
Tracking Accuracy (%)	97.1	98.0	98.6	99.2
Response Time (S)	0.25	0.21	0.18	0.14
Efficiency (%)	93.4	94.5	95.2	96

Table V shows that all simulation settings, converter topology, and operating circumstances are maintained constant, with only the MPPT algorithm changing. The suggested COA-RBFNN consistently outperforms standard MPPT algorithms in terms of convergence speed, tracking accuracy, and conversion efficiency. These findings suggest that the observed performance gain is due to the COA-based optimisation of the RBFNN rather than the converter topology alone.

TABLE VI
Tracking performance efficiency under various literature

MPPT strategies	Response time (s)	Tracking accuracy (%)
ABC [19]	0.16	98.41
HPIO [21]	0.30	99.08
Proposed	0.14	99.2

The table's data in Table VI proves that presented model performs the best overall. With the fastest response time of 0.14s and highest tracking accuracy of 99.2%, it is the best option. The usefulness and dependability of proposed method are confirmed by its faster response time and more accurate tracking when compared to ABC and HPIO**.**

IV. Conclusion

The proposed framework uses an interleaved DuoCore high-gain converter and a COA-tuned RBFNN-based MPPT for grid applications. With less ripple, the interleaved DuoCore high-gain converter increases the PV output, while COA-RBFNN based MPPT performs better tracking model from PV. The BDC converter effectively controls battery charging and discharging to provide constant energy balance. The PI-controlled three-phase VSI controls both active and reactive power helps to further ensure dependable grid synchronisation. A 96% power conversion efficiency and a 99.2% tracking accuracy are attained from the validation in MATLAB/Simulink, indicating better performance than current approaches. Its practical potential can also be confirmed by expanding the system for widespread use in microgrids and EV charging infrastructure in further studies.

References

[1] K. Swamynathan, N. Mahalingam, A. Paramasivam, and S. Vijayalakshmi, "PV based OFF grid charging station for E-vehicles using PWM and phase shift controlled interleaved three port converter," *SN Applied Sciences*, vol. 5, no. 12, pp. 331, Dec. 2023. https://doi.org/10.1007/s42452-023-05571-w.

[2] S. Karlilar Pata, and M. Balcilar, "Decarbonizing energy: Evaluating fossil fuel displacement by renewables in OECD countries, *Environmental Science and Pollution Research*, vol. 31, no. 21, pp. 31304-31313, 2024.

[3] B. U. D. Abdullah, S. L. Dhar, S. P. Jaiswal, M. M. Gulzar, M. Alqahtani, and M. Khalid, “Hybrid MPPT control using hybrid pelican optimization algorithm with perturb and observe for PV connected grid,” *Frontiers in Energy Research*, vol. 12, pp. 1505419, Jan. 2025. https://doi.org/10.3389/fenrg.2024.1505419.

[4] S. M. Belhadj, B. Meliani, H. Benbouhenni, I. Colak, Z. M. S. Elbarbary, and S. F. Al-Gahtani, “Control of three-level quadratic DC-DC boost converters for energy systems using various technique-based MPPT methods,” *Scientific Reports*, vol. 15, no. 1, pp. 14631, Apr. 2025. https://doi.org/10.1038/s41598-025-99551-2.

[5] S. Khan, M. Zaid, M. M. A. Khan, and A. Sarwar, “A non-pulsating input current step-up DC/DC converter with common ground structure for photovoltaic applications,” *IEEE Access*, vol. 9, pp. 159432-159446, Nov. 2021. https://doi.org/10.1109/ACCESS.2021.3128255.

[6] M. L. Alghaythi, R. M. O’Connell, N. E. Islam, M. M. S. Khan, and J. M. Guerrero, “A high step-up interleaved DC-DC converter with voltage multiplier and coupled inductors for renewable energy systems,” *IEEE Access*, vol. 8, pp. 123165-123174, Jul. 2020. https://doi.org/10.1109/ACCESS.2020.3007137.

[7] S. W. Seo, J. H. Ryu, Y. Kim, and H. H. Choi, “Non-isolated high step up DC/DC converter with coupled inductor and switched capacitor,” *IEEE Access*, vol. 8, pp. 217108217122, Dec. 2020. https://doi.org/10.1109/ACCESS.2020.3041738.

[8] Y. Zheng, B. Brown, W. Xie, and S. Li, “High step-up DCDC converter with zero voltage switching and low input current ripple,” *IEEE Transactions on Power Electronics*, vol. 35, no. 9, pp. 94169429, Jan. 2020. https://doi.org/10.1109/TPEL.2020.2968613.

[9] V. Abbasi, S. Rostami, S. Hemmati, and S. Ahmadian, “Ultrahigh step-up quadratic boost converter using coupled inductors with low voltage stress on the switches,” *IEEE Journal of Emerging and Selected Topics in Power Electronics*, vol. 10, no. 6, pp. 7733-7743, Aug. 2022. https://doi.org/10.1109/JESTPE.2022.3195817.

[10] S. Pirpoor, S. Rahimpour, M. Andi, N. Kanagaraj, S. Pirouzi, and A. H. Mohammed, “A novel and high-gain switched-capacitor and switched-inductor-based DC/DC boost converter with low input current ripple and mitigated voltage stresses,” *IEEE Access* 10, pp. 32782-32802, Mar. 2022. 10.1109/ACCESS.2022.3161576.

[11] G. Tsolaridis, M. Jeong, and J. Biela, “Evaluation of current control structures for multi-phase interleaved DC-DC converters,” *IEEE Access*, vol. 9, pp. 142616-142631, Oct. 2021. https://doi.org/10.1109/ACCESS.2021.3121060.

[12] A. Rajulapati, and P. Mahalingam, “High gain multi-input converter with inherent current sharing mechanism for photovoltaic applications,” *Solar Energy*, vol. 233, pp. 118-133, Feb. 2022. https://doi.org/10.1016/j.solener.2022.01.028.

[13] K. S. Kavin, and P. Subha Karuvelam, “PV-based grid interactive PMBLDC electric vehicle with high gain interleaved DC-DC SEPIC Converter,” *IETE Journal of Research*, vol. 69, no. 7, pp. 4791-4805, Sep. 2023. https://doi.org/10.1080/03772063.2021.1958070.

[14] S. Nagaraja Rao, S. K. Anisetty, B. M. Manjunatha, B. M. Kiran Kumar, V. Praveen Kumar, and S. Pranupa, “Interleaved high-gain boost converter powered by solar energy using hybrid-based MPP tracking technique,” *Clean Energy*, vol. 6, no. 3, pp. 460-475, Jun. 2022. https://doi.org/10.1093/ce/zkac026.

[15] K. S. Kavin, P. Subha Karuvelam, M. Devesh Raj, and M. Sivasubramanian, “A novel KSK converter with machine learning MPPT for PV applications,” *Electric power components and systems*, pp. 1-19, Apr. 2024. https://doi.org/10.1080/15325008.2024.2346806.

[16] S. R. Kiran, C. H. Basha, V. P. Singh, C. Dhanamjayulu, B. R. Prusty, and B. Khan, “Reduced simulative performance analysis of variable step size ANN based MPPT techniques for partially shaded solar PV systems,” *IEEE access*, vol. 10, pp. 48875-48889, May 2022. https://doi.org/10.1109/ACCESS.2022.3172322.

[17] Y. Türkay, and A. G. Yüksek, “Investigating The Potential of An ANFIS Based Maximum Power Point Tracking Controller for Solar Photovoltaic Systems,” *IEEE Access*, Mar. 2025. https://doi.org/10.1109/ACCESS.2025.3547954.

[18] A. M. Eltamaly, H. M. Farh, and A. G. Abokhalil, “A novel PSO strategy for improving dynamic change partial shading photovoltaic maximum power point tracker,” *Energy sources, part a: recovery, utilization, and environmental effects*, vol. 46, no. 1, pp. 8736-8750, Dec. 2024. https://doi.org/10.1080/15567036.2020.1769774.

[19] C. González-Castaño, C. Restrepo, S. Kouro, and J. Rodriguez, “MPPT algorithm based on artificial bee colony for PV system,” *IEEE Access*, vol. 9, pp. 43121-43133, Mar. 2021. https://doi.org/10.1109/ACCESS.2021.3066281.

[20] C. Restrepo, N. Yanẽz-Monsalvez, C. González-Castaño, S. Kouro, and J. Rodriguez, “A fast converging hybrid mppt algorithm based on abc and p&o techniques for a partially shaded pv system,” Mathematics, vol. 9, no. 18, pp. 2228, Sep. 2021. https://doi.org/10.3390/math9182228.

[21] Z. Zhao, M. Zhang, Z. Zhang, Y. Wang, R. Cheng, J. Guo, P. Yang, C. S. Lai, P. Li, and L. L. Lai, “Hierarchical pigeon-inspired optimization-based MPPT method for photovoltaic systems under complex partial shading conditions,” *IEEE Transactions on Industrial Electronics*, vol. 69, no. 10, pp. 10129-10143, Dec. 2021. https://doi.org/10.1109/TIE.2021.3137595.

S. Suganya is an accomplished academician and researcher in the field of Electrical and Electronics Engineering, currently serving as an Assistant Professor at Paavai Engineering College, Namakkal. She received her Ph.D. in Energy Engineering from Anna University in 2024, with her research focusing on advanced electrode materials and high-performance energy storage systems. She holds an M.E. in Power Systems Engineering and a B.E. in Electrical and Electronics Engineering. With over 14 years of combined teaching and industry experience, her areas of expertise include energy storage systems, renewable energy integration, electric vehicles, power electronics, smart grid technologies, and intelligent control techniques. She has published several research papers in reputed national and international journals and holds 12 published patents. Dr. Suganya is a Life Member of the Institution of Engineers (India). Her work integrates theoretical knowledge with practical applications, contributing significantly to sustainable energy technologies and engineering education.

S. Thirunavukkarasu received his B.E degree in Electrical and Electronics Engineering from Sona College of Technology, Periyar University, Salem in the year of 2003 and M.E degree in Power Electronics and Drives from Sri Ramakrishna Engineering College, Anna University, Chennai in the year of 2005. He was completed Ph.D. degree in Electrical Engineering from Anna University, Chennai in the year of 2020 and he is currently working as an Associate professor in the department of Electrical and Electronics Engineering, Paavai Engineering College, Namakkal. His area of research interests are power electronics and drives, control system, power quality.

S. Siddik earned his Bachelor's degree in Electrical Engineering from the University of Madras, Chennai, in 1997. He later completed his Master of Engineering (M.E.) in Power System Engineering in 2013 and his Doctor of Philosophy (Ph.D.) in Electrical Engineering from Anna University, Chennai, in 2023. He is currently serving as an Assistant Professor in the Department of Electrical and Electronics Engineering at Paavai Engineering College, Namakkal. His research interests include power systems, renewable energy conversion systems, embedded system applications, smart grid intelligent systems, and generative AI.

C. Arulkumar is a distinguished academician with a strong background in Electrical Engineering. He graduated from Anna University, Chennai, and obtained his M.E. degree in Power Electronics and Drives in 2008, followed by a Ph.D. in Electrical Engineering in 2021. He is a Member of the Institution of Engineers (India) (IEI) and the Indian Society for Technical Education (ISTE). He currently serves as an Associate Professor in the Department of Electrical and Electronics Engineering at Paavai Engineering College, Namakkal. His areas of expertise include Power Electronic Converters, Renewable Energy Applications, Smart Grid Integration, and Image Processing Techniques. He is deeply committed to advancing research and contributing to the development of these emerging and interdisciplinary fields.